

Towards Magnon Valleytronics

Doried Ghader

College of Engineering and Technology, American University of the Middle East, Eqaila, Kuwait

Valleytronics is a pioneering technological field relying on the fermionic valley degree of freedom to achieve novel electronic functionality. Topological valley-projected electronic states confined to domain walls in bilayer graphene were extensively studied in view of their potentials in valleytronics. Here, we study the magnonic version of domain wall states in ferromagnetic bilayers characterized by Dzyaloshinskii-Moriya interaction and uniform layer-dependent electrostatic doping. In particular, we explore topological confinement of magnon modes on layer stacking domain walls separating two semi-infinite ferromagnetic regions with AB and BA stacking. We predict that layer-dependent electrostatic doping induces a pair of valley-projected chiral boundary modes that admit topological interpretation. We conclude that magnon valley index can constitute an additional degree of freedom for 2D magnonic applications.

The recent realization of two-dimensional (2D) materials with intrinsic magnetism [1, 2] constitutes an important breakthrough in condensed matter physics. This discovery immediately stimulated tremendous interest in the fundamental physics underlying 2D magnets, as well as their technological potentials [3-22]. With the novel characteristics of their magnetic excitations, 2D magnets are expected to open new horizons in technological fields like magnonics.

The magnon spectrum in 2D honeycomb ferromagnets mimic the electronic band structure of graphene [11], with Dirac cones at the corners of the hexagonal Brillouin zone (BZ). Similar to graphene, the Dirac spectrum of 2D magnons in honeycomb ferromagnets is characterized by 2 non-equivalent valleys K and $K' = -K$. The energy degeneracy at valleys is protected by inversion and time reversal symmetries. Next-nearest-neighbor Dzyaloshinskii-Moriya interaction (DMI), present in several 2D ferromagnets, breaks the inversion symmetry and opens topological gaps at $\pm K$. In bilayer ferromagnets, the valley gap can also be induced by layer-dependent electrostatic doping [23]. A recent study [24] predicts that inversion symmetry breaking by electrostatic doping can generate topological magnon valley currents in quasi-infinite ferromagnetic bilayers (FBL).

The valley degree of freedom in electronic systems is proved very promising for quantum technologies, leading to the novel technological field of valleytronics [25–38]. In particular, topological confinement of electronic states on domain walls of bilayer graphene (BLG) has been proposed to realize novel nano-electronic devices, like valley filters and valves. Applying a

perpendicular electric field in BLG breaks inversion symmetry and consequently opens a valley band gap [39-43] that admits a topological interpretation [26, 44]. Whilst the integral of the Berry curvature over the full BZ is zero, the Berry integral within a single valley is nonzero resulting in a valley-projected topological index [26, 27, 46-49]. Novel domain walls can then be formed in BLG by a sign reversal of the perpendicular electric field. Analysis of the sub-gap electronic states near $\pm K$ valleys demonstrates the existence of two topologically protected chiral modes confined to the electric-field domain wall (EFW). Domain walls can also be formed in BLG by interlayer stacking reversal, where the layer stacking switches from AB to BA configurations. In the presence of a uniform interlayer electric field, layer stacking domain walls (LSW) also support topological chiral modes, analogous to their EFW counterparts. The technological interest in the valley degree of freedom was extended to 2D photonic [50] and phononic [51] crystals. Magnon valleytronics, however, did not yet receive the deserved attention.

In this work, we study magnon topological confinement in LSW embedded in a 2D ferromagnetic bilayer (FBL). The theoretical study is based on a four-band continuum model, developed near $\pm K$ valleys, including weak DMI and uniform layer-dependent electrostatic doping (ED). The four-band continuum Hamiltonian of FBLs does not have a fermionic counterpart, and is hence a candidate for new physics not present in 2D electron systems. For zero DMI and uniform ED, we find that the LSW confines topologically protected chiral 1D magnon modes analogous to their fermionic counterpart. In addition, we observe flat energy magnon modes localized on the LSW that are absent in fermionic systems. Introducing weak DMI results in a topologically compensated LSW, and the intragap magnon spectrum becomes completely gapped. These prediction of 1D magnon modes on LSW shall constitute an important step towards magnon valleytronics.

The four-band magnon Hamiltonian, $\mathcal{H}_{AB}^{\pm K}$, for an infinite AB-stacked FBL near $\pm K$ valleys can be expressed as [6, 24]

$$\mathcal{H}_{AB}^{\pm K} = JS \begin{pmatrix} 3 + v_0 - U + m & v(\pm p_x - ip_y) & 0 & -v_0 \\ v(\pm p_x + ip_y) & 3 - U - m & 0 & 0 \\ 0 & 0 & 3 + U + m & v(\pm p_x - ip_y) \\ -v_0 & 0 & v(\pm p_x + ip_y) & 3 + v_0 + U - m \end{pmatrix}$$

Here $v_0 = J_{\perp}/J$, $m = 3\sqrt{3}D/J$, and $v = \sqrt{3}/2$. The coefficients J and J_{\perp} denote the nearest neighbor intra and interlayer exchange coefficients respectively. S denotes spin, D is the DMI coefficient, U represents the layer-dependent electrostatic doping potential (normalized by JS). p_x and p_y are the momenta along x and y directions. As stated previously, due to the presence of v_0 and m on the diagonal, $\mathcal{H}_{AB}^{\pm K}$ does not have an electronic analogue.

For an infinite BA-stacked FBL, the equivalent Hamiltonian reads

$$\mathcal{H}_{BA}^{\pm K} = JS \begin{pmatrix} 3 - U + m & v(\pm p_x - ip_y) & 0 & 0 \\ v(\pm p_x + ip_y) & 3 + v_0 - U - m & -v_0 & 0 \\ 0 & -v_0 & 3 + v_0 + U + m & v(\pm p_x - ip_y) \\ 0 & 0 & v(\pm p_x + ip_y) & 3 + U - m \end{pmatrix}$$

We next consider a 2D bilayer ferromagnet with an LSW (at $x = 0$) separating two semi-infinite regions, with AB and BA stacking in the regions $x > 0$ and $x < 0$ respectively. The corresponding four-components magnon wavefunctions in the regions $x \geq 0$ are denoted ψ^\pm respectively, with $\psi^\pm = \{\phi_i^\pm, i = 1, \dots, 4\}$. The translational symmetry in the system is broken (preserved) along the x - direction (y - direction). The behavior of ψ^\pm is hence dictated by the functional form $e^{-\lambda x} e^{ip_y}$, where $\lambda = \alpha + i\beta$ denotes the generalized phase factor in the x - direction [15, 18, 20, 21, 26, 27]. For intragap modes confined to the LSW, λ is real and the wavefunction decays exponentially away from the LSW.

Reinstating the momenta as differential operators in $\mathcal{H}_{AB}^{\pm K}$ (equivalently $\mathcal{H}_{BA}^{\pm K}$), the wave equation $(\mathcal{H}_{AB}^{\pm K} - \epsilon I)\psi = 0$ yields four real solutions for λ , namely

$$\lambda_{1(2)}^\pm = \pm \sqrt{p_y^2 - \frac{a + (-)b}{v^2}}$$

with

$$a = 9 - m^2 + \Omega^2 + 3v_0 - \Omega(6 + v_0) + U^2$$

$$b = \sqrt{(-3 + \Omega)[(-3 + \Omega)v_0^2 + 4(-3 + \Omega)U^2 - 4v_0U(m + U)]}$$

We have also defined $\Omega = \frac{\epsilon}{JS}$. The solutions $\lambda_{1(2)}^\pm$ are adopted for ψ^\pm respectively, and the components ϕ_i^\pm are written as $\phi_i^\pm = u_{i1}e^{-\lambda_1^\pm x} e^{ip_y} + u_{i2}e^{-\lambda_2^\pm x} e^{ip_y}$. This generate 16 coefficients, $\{u_{ij}; i = 1, \dots, 4, j = 1, 2\}$, to be determined via boundary conditions derived from the matching method [26, 27, 52-56]. To be specific, 16 boundary conditions can be derived by matching the wavefunctions components ϕ_i^\pm and their derivatives across the LSW. First, the magnon wavefunction is required to be continuous across the domain wall, resulting in 4 boundary equations $\phi_i^+(x = 0^+) = \phi_i^-(x = 0^-)$. The remaining 12 boundary equations are derived by

matching the rows of the K valley wave equations $(\mathcal{H}_{AB}^K - \epsilon I)\psi^> = 0$ and $(\mathcal{H}_{AB}^K - \epsilon I)\psi^< = 0$ across the LSW. First rows yield

$$v_0\phi_1^+ - iv(\partial_x\phi_2^+ - \partial_x\phi_2^-) - v_0\phi_4^+ = 0$$

$$(2 + U - \Omega)(\partial_x\phi_1^+ - \partial_x\phi_1^-) + v_0(\partial_x\phi_1^+ - \partial_x\phi_4^+) - ivp_y(\partial_x\phi_2^+ - \partial_x\phi_2^-) - iv(\partial_x^2\phi_2^+ - \partial_x^2\phi_2^-) = 0$$

$$(2 + U - \Omega)(\partial_x^2\phi_1^+ - \partial_x^2\phi_1^-) + v_0(\partial_x^2\phi_1^+ - \partial_x^2\phi_4^+) - ivp_y(\partial_x^2\phi_2^+ - \partial_x^2\phi_2^-) - iv(\partial_x^3\phi_2^+ - \partial_x^3\phi_2^-) = 0$$

The first equation is determined by subtracting the first-row equations. Applying ∂_x and ∂_x^2 on these rows, followed by subtraction, yield the remaining two equations. The rest of the rows yield 9 additional equations which completes the set to 16.

Substituting $\phi_i^\pm = u_{i1}e^{-\lambda_1^\pm x}e^{ip_y} + u_{i2}e^{-\lambda_2^\pm x}e^{ip_y}$ in the derived boundary conditions yields a 16×16 linear system, $M|u\rangle = 0$. The dispersion relations, $\Omega(p_y)$, for the intragap magnon modes are then determined by solving the determinant equation $|M(p_y, \Omega)| = 0$. We succeeded in reducing the determinant equation, which boils down to

$$(c_1\lambda_1^+ + c_2\lambda_2^+ + c_{12}\lambda_1^+\lambda_2^+ + c_0)(c_1\lambda_1^+ + c_2\lambda_2^+ - c_{12}\lambda_1^+\lambda_2^+ - c_0) = 0$$

with

$$c_{1(2)} = vv_0[-9 + 3a + m^2 - U^2 - 2p_y^2v^2 - 6v_0 - (+)b - (+)\Omega(6 - e + 2v_0)]$$

$$c_{12} = v^2(2p_y^2v^2 - 2a)$$

This development allows us to determine the magnon propagating and confined modes in the FBL system, composed of local AB and BA stacking regions separated by a domain wall. Figure 1 presents numerical results near the K valley, for selected electrostatic doping potential and negligible DMI. The shaded regions represent the continuous bulk magnon spectrum which differs significantly from the electronic structure of BLG. The red dispersion curves correspond to the magnon modes confined to the LSW. The bulk spectrum profile allows the presence of a boundary flat energy mode, absent in BLG with embedded LSW or EFW. More important, the numerical results in figure 1 demonstrate the existence of pairs of valley intragap chiral magnon modes, confined to the LSW, and propagating in opposite velocities at the $\pm K$ valleys. We can readily

draw a topological interpretation for these modes, in analogy with their fermionic counterparts [27]. Magnon valley Berry curvatures, Hall conductivity and Chern numbers are indeed well defined in FBLs with layer-dependent electrostatic doping [24], and the presence of the magnon chiral modes is associated with the change in the valley Chern number sign across the LSW [27].

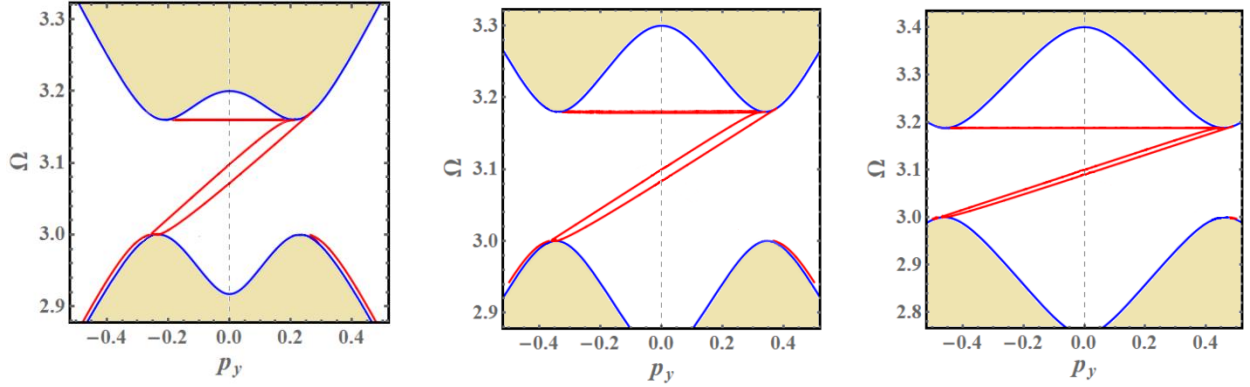


Figure 1: Continuous magnon bulk spectrum (shaded region) near the K – valley and domain wall magnon modes (red) for zero DMI and uniform doping potential U . We set $J = 1$ and $v_0 = 0.2$ in all figures. The potential U takes the values 0.2, 0.3 and 0.4 in the left, middle and right figures respectively. The numerical results demonstrate the existence of a flat energy boundary mode and a pair of topologically protected intragap chiral modes.

In figure 2, we investigate the effect of a weak DMI on the LSW confined modes. In the presence of DMI, the LSW is topologically compensated and the LSW spectrum near $\pm K$ valleys is completely gapped. This is analogous to the compensated domain wall in BLG separating two regions with reversed interlayer electric field and layer stacking [27].

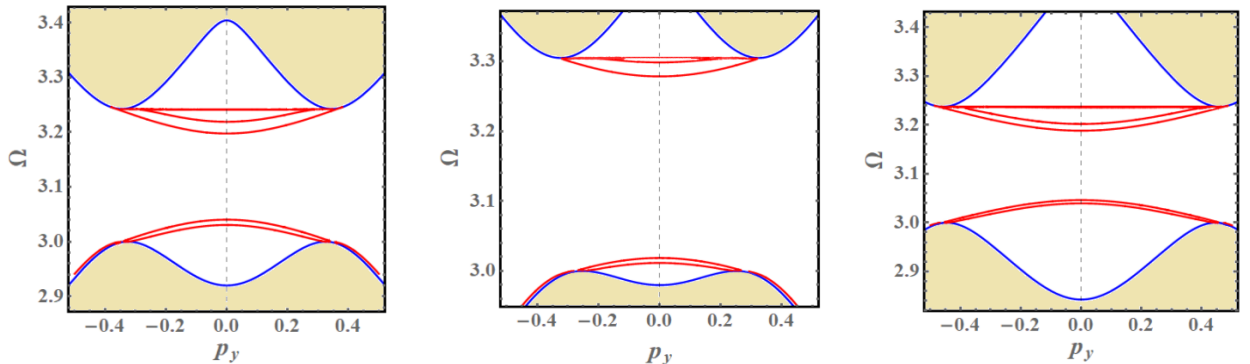


Figure 2: The bulk and boundary magnon spectra in the presence of a weak DMI. The parameters are *left* ($U = 0.3, D = 0.02J$), *middle* ($U = 0.3, D = 0.04J$) and *right* ($U = 0.4, D = 0.02J$). In all figures, $J = 1$ and $v_0 = 0.2$.

Discussion- This work constitutes an important step towards magnon valleytronics utilizing magnon modes confined to LSW in FBL. We demonstrate that LSW in FBL with negligible DMI and uniform ED binds a pair of gapless valley-projected chiral magnon modes. Similar to their fermionic counterparts, the predicted chiral magnon modes admit a topological interpretation in term of the variation of the magnon valley index across the LSW. The magnon valley index hence serve as a good quantum number offering an additional degree of freedom promising for magnonic applications. Topologically confined 1D magnon modes on domain walls might have significant advantages over edge modes in nanoribbons, as their realization might be less challenging. Since the chiral valley modes propagate in opposite directions at the $\pm K$ valleys, LSW can serve to realize magnon valley filters and valves [26], indispensable for magnonic circuitry. Given their topological protection, damping of these modes should be negligible. With the rapid advancement in the experimental techniques to fabricate and characterize 2D magnetic materials, experimental testing of our predictions shall be feasible.

References

- [1] Gong, C. et al. Discovery of intrinsic ferromagnetism in two-dimensional Van der Waals crystals, *Nature* **546**, 265 (2017).
- [2] Huang B. et al. Layer-dependent ferromagnetism in a Van der Waals crystal down to the monolayer limit, *Nature* **546**, 270 (2017).
- [3] Cheng, R., Okamoto, S. & Xiao, D. Spin Nernst effect of magnons in collinear antiferromagnets, *Phys. Rev. Lett.* **117**, 217202 (2016)
- [4] Zyuzin, V. A. & Kovalev, A. A. Magnon Spin Nernst Effect in Antiferromagnets, *Phys. Rev. Lett.* **117**, 217203 (2016)
- [5] Owerre, S. A. A first theoretical realization of honeycomb topological magnon insulator, *J. Phys.: Condens. Matter* **28**, 386001 (2016)
- [6] Owerre, S. A. Magnon Hall effect in AB-stacked bilayer honeycomb quantum magnets, *Phys. Rev. B* **94**, 094405 (2016)
- [7] Nakata, K., Klinovaja, J. & Loss, D. Magnonic quantum Hall effect and Wiedemann-Franz law, *Phys. Rev. B* **95**, 125429 (2017)
- [8] Shiomi, Y., Takashima, R. and Saitoh, E. Experimental evidence consistent with a magnon Nernst effect in the antiferromagnetic insulator $MnPS_3$, *Phys. Rev. B* **96**, 134425 (2017)
- [9] Owerre, S. A. Dirac Magnon Nodal Loops in Quasi-2D Quantum Magnets, *Sci. Rep.* **7**, 6931 (2017)
- [10] Lado, J. L. & Fernández-Rossier, J. On the origin of magnetic anisotropy in two dimensional CrI_3 , *2D Materials* **4**, 035002 (2017).

- [11] Pershoguba, S. S., Banerjee, S., Lashley, J. C., Park, J., Ågren, H., Aeppli, G. & Balatsky, A.V. Dirac magnons in honeycomb ferromagnets, *Phys. Rev. X* **8**, 011010 (2018)
- [12] Lee, K. H., Chung, S. B. Park, K. & Park, J.-G. Magnonic quantum spin Hall state in the zigzag and stripe phases of the antiferromagnetic honeycomb lattice, *Phys. Rev. B* **97**, 180401(R) (2018)
- [13] Jin, W. et al. Raman fingerprint of two terahertz spin wave branches in a two-dimensional honeycomb Ising ferromagnet, *Nat. Comm.* **9**, 5122 (2018)
- [14] Chen, L. et al. Topological spin excitations in honeycomb ferromagnet CrI_3 , *Phys. Rev. X* **8**, 041028 (2018)
- [15] Pantaleón, P. A. & Xian, Y. Effects of edge on-site potential in a honeycomb topological magnon insulator, *J. Phys. Soc. Japan* **87**, 064005 (2018)
- [16] Xing, X. W. et al. Magnon Transport in Quasi-Two-Dimensional van der Waals Antiferromagnets, *Phys. Rev. X* **9**, 011026 (2019)
- [17] Owerre, S. A. Magnonic Floquet Quantum Spin Hall Insulator in Bilayer Collinear Antiferromagnets, *Sci. Rep.* **9**, 7197 (2019)
- [18] Ghader, D. & Khater, A. Discretized dynamics of exchange spin wave bulk and edge modes in honeycomb nanoribbons with armchair edge boundaries, *J. Phys.: Condens. Matter* **31**, 315801 (2019)
- [19] Ghader, D. & Khater, A. Theory for the spin dynamics in ultrathin disordered binary magnetic alloy films: application to cobalt-gadolinium, *JMMM* **482**, 88-98 (2019)
- [20] Ghader, D. & Khater, A. Asymmetric dynamics of edge exchange spin waves in honeycomb nanoribbons with zigzag and bearded edge boundaries, *Sci. Rep.* **9**, 6290 (2019)
- [21] Ghader, D. & Khater, A. A new class of nonreciprocal spin waves on the edges of 2D antiferromagnetic honeycomb nanoribbons, *Sci. Rep.* **9**, 15220 (2019)
- [22] Ghader, D. Magnon magic angles and tunable Hall conductivity in 2D twisted ferromagnetic bilayers, arXiv:1911.07009 (2019)
- [23] Jiang, S., Li, L., Wang, Z., Mak, K. F., & Shan, J. Controlling magnetism in 2D CrI_3 by electrostatic doping, *Nat. Nanotechnol.* **13**, 549 (2018)
- [24] Zhai, X. & M. Blanter, Y. M. Topological valley transport of gapped Dirac magnons in bilayer ferromagnetic insulators, arXiv:2002.00446 (2020)
- [25] Rycerz, A., Tworzydło, J. & Beenakker, C. W. J. Valley filter and valley valve in graphene *Nat. Phys.* **3**, 172 (2007)
- [26] Martin, I., Blanter, Y. M. & Morpurgo, A. F. Topological confinement in bilayer graphene, *PRL* **100**, 036804 (2008)
- [27] Zhang, F., MacDonald, A. H. & Mele, E. J. Valley Chern numbers and boundary modes in gapped bilayer graphene, *PNAS* **110**, (26) 10546-10551 (2013)

- [28] Alden, J. S. et al. Strain solitons and topological defects in bilayer graphene, PNAS **110**, (28) 11256-11260 (2013)
- [29] Vaezi, A., Liang, Y., Ngai, D. H., Yang, L. & Kim, E.-A. Topological Edge States at a Tilt Boundary in Gated Multilayer Graphene, Phys. Rev. X **3**, 021018 (2013)
- [30] Mak, K. F., McGill, K. L., Park, J., & McEuen, P. L. The valley Hall effect in MoS_2 transistors, Science **344**, 1489 (2014)
- [31] Xu, X., Yao, W., Xiao, D. & Heinz, T. F. Spin and pseudospins in layered transition metal dichalcogenides, Nat. Phys. **10**, **343** (2014)
- [32] Pan, H., Li, Z., Liu, C.-C., Zhu, G., Qiao, Z., & Yao, Y. Valley-polarized quantum anomalous Hall effect in silicene, Phys. Rev. Lett. **112**, 106802 (2014)
- [33] Long, J. et al. Topological valley transport at bilayer graphene domain walls, Nature, **520**, 650–655 (2015)
- [34] Shaibely, J. R. et al. Valleytronics in 2D materials, Nat. Rev. Mater. **1**, 16055 (2016).
- [35] Ang, Y. S., Yang, S. A., Zhang, C., Ma, Z. & Ang, L. K. Valleytronics in merging Dirac cones: all-electric-controlled valley filter, valve, and universal reversible logic gate, Phys. Rev. B **96**, 245410 (2017)
- [36] Bussolotti, F. et al. Roadmap on finding chiral valleys: screening 2D materials for valleytronics, Nano Futures, **2**, 032001 (2018)
- [37] Vitale, S. A. et al. Valleytronics: opportunities, challenges, and paths forward, Small **14**, 1801483 (2018).
- [38] Niu, Z. Spin-valley filter effect and Seebeck effect in a silicene based antiferromagnetic/ferromagnetic junction, New J. Phys. **21**, 093044 (2019)
- [39] McCann, E. & Fal'ko, V. I., Landau-level degeneracy and quantum Hall effect in a graphite bilayer, Phys. Rev. Lett. **96**, 086805 (2006)
- [40] Ohta, T., Bostwick, A., Seyller, T., Horn, K., & Rotenberg, E. Controlling the electronic structure of bilayer graphene, Science **313**, 951–954 (2006)
- [41] Oostinga, J. B., Heersche, H. B., Liu, X., Morpurgo, A. F., & Vandersypen, L. M. K. Gate-induced insulating state in bilayer graphene devices. Nat Mater **7**, 151–157 (2008)
- [42] Castro, E. V. et al. Biased bilayer graphene: Semiconductor with a gap tunable by the electric field effect, Phys Rev Lett **99**, 216802 (2007)
- [43] Zhang, F., Sahu, B., Min, H., & MacDonald, A. H. Band structure of ABC-stacked graphene trilayers, Phys Rev B **82**, 035409 (2010)
- [44] Zhang, F., Jung, J., Fiete, G. A., Niu, Q., & MacDonald, A. H. Spontaneous quantum Hall states in chirally stacked few-layer graphene systems. Phys Rev Lett **106**, 156801 (2011)
- [45] Li J, Morpurgo AF, Büttiker M, & Martin I (2010) Marginality of bulk-edge correspondence for single-valley Hamiltonians. Phys Rev B **82**:245404.

- [46] Li, J., Martin, I., Buttiker, M., & Morpurgo, A. F. Topological origin of sub-gap conductance in insulating bilayer graphene, *Nat Phys* **7**, 38–42 (2011)
- [47] Qiao, Z., Jung, J., Niu, Q., & Macdonald, A. H. Electronic highways in bilayer graphene, *Nano Lett* **11**, 3453–3459 (2011)
- [48] Jung, J., Zhang, F., Qiao, Z., & MacDonald, A. H. Valley-Hall kink and edge states in multilayer graphene, *Phys Rev B* **84**, 075418 (2011)
- [49] Zarenia, M., Pereira, J.M., Farias, G. A., & Peeters, F.M. Chiral states in bilayer graphene: Magnetic field dependence and gap opening, *Phys Rev B* **84**, 125451 (2011)
- [50] Noh, J., Huang, S., Chen, K. P., & Rechtsman, M. C., Observation of Photonic Topological Valley Hall Edge States, *Phys. Rev. Lett.* **120**, 063902 (2018).
- [51] Lu, J., Qiu, C., Deng, W., Huang, X., Li, F., Zhang, F., Chen, S., & Liu, Z., Valley topological phases in bilayer sonic crystals, *Phys. Rev. Lett.* **120**, 116802 (2018)
- [52] Ghader, D., Ashokan, V., Ghantous, M. A. & Khater, A. Spin waves transport across a ferrimagnetically ordered nanojunction of cobalt-gadolinium alloy between cobalt leads, *Eur. Phys. J. B* **86**, 180 (2013)
- [53] Ashokan, V., Ghantous, M. A., Ghader, D. & Khater, A., Ballistic transport of spin waves incident from cobalt leads across cobalt–gadolinium alloy nanojunctions, *JMMM* **363**, 66-76 (2014)
- [54] Ashokan, V., Khater, A., Ghantous, M. A. & Ghader, D. Spin wave ballistic transport properties of $[Co_{1-c}Gd_c]_{\ell'}[Co]_{\ell}[Co_{1-c}Gd_c]_{\ell'}$ nanojunctions between Co leads, *JMMM* **384**, 18-26 (2015)
- [55] Ashokan, V., Ghantous, M. A., Ghader, D. & Khater, A. Computation of magnons ballistic transport across an ordered magnetic iron-cobalt alloy nanojunction between iron leads, *Thin Solid Films* **616**, 6-16 (2016)
- [56] Khater, A., Saim, L., Tigrine, R. & Ghader, D. Fabry–Perot magnonic ballistic coherent transport across ultrathin ferromagnetic lamellar bcc Ni nanostructures between Fe leads, *Surf. Sci.* **672**, 47 (2018)